J. Fluid Mech. (1988), *vol.* 187, *pp.* 373–394
Printed in Great Britain

Vertical and lateral turbulent dispersion: some experimental results

By R. I. NOKES
Research School of Earth Sciences, Australian National University, Canberra, Australia

AND I. R. WOOD
Civil Engineering Department, University of Canterbury, Christchurch, New Zealand

(Received 21 July 1986 and in revised form 29 July 1987)

The results of an experimental programme designed to investigate turbulent dispersion of a continuous contaminant source in a wide channel are presented. Both two-dimensional vertical dispersion and the determination of the lateral diffusion coefficient are described. The eigenfunction solution to the turbulent diffusion equation, presented in Nokes *et al.* (1984) and discussed in greater detail in Nokes (1985), is strongly supported by the results of vertical mixing described here. A variety of source locations are examined in this study and the location of the ideal source, predicted by theory, is verified by the experimental results. For the two smooth-bed flows investigated the depth-averaged values of ϵ_z, deduced from the rates of lateral spreading of the plume, lie at the lower end of the range of values obtained by other researchers. Considering only the results obtained in wide channels, the authors demonstrate that previously published values of the lateral diffusion coefficient, non-dimensionalized by the shear velocity u_* and the flow depth d are independent of all flow parameters except the friction factor $f = 8u_*^2/\bar{u}^2$ where $\bar{u}$ is the mean velocity in the flow. Indeed, above a value of $f = 0.055$ $\epsilon_z/u_* d$ is also found to be independent of f, and takes a value of 0.134. A brief mathematical analysis of the three-dimensional mixing processes in the near-source region is presented, and utilized to investigate the coupling between the lateral and vertical diffusion processes in this region. Based on these mathematical arguments the experimental results imply that the vertical and lateral diffusion processes are essentially uncoupled in the near-source zone, and thus the lateral diffusivity and longitudinal velocity have similar vertical dependence.

1. Introduction

Two aspects of the turbulent dispersion of a neutrally buoyant contaminant, released continuously into a channel, are of real interest. Of primary importance is lateral spreading, as this is the predominant feature of the mixing process in wide natural channels. In order to predict the impact of an effluent source on a given channel it is important that the engineer be able to estimate the rate at which the effluent is diluted to acceptable levels. This dilution rate is determined solely by the characteristics of the lateral mixing process. The extreme complexity of the mixing processes in natural channels, which include irregular mean and turbulent motions generated by changing channel geometry, makes it necessary to oversimplify any theoretical description of the system. Even for the controlled environment of a straight, rectangular laboratory flume no theoretical basis exists for the prediction

of the lateral mixing rates, even though turbulence, generated by the channel boundaries, vertical velocity shear and perhaps secondary currents are the only mixing mechanisms present. Therefore, these mixing rates and their dependence on the various flow parameters (Froude number, Reynolds number, aspect ratio etc.) must be determined from experiment. The progress made in this direction is discussed in §1.1.

Although of less practical importance, the vertical mixing process is also of interest to theoreticians and experimentalists alike. Vertical turbulent diffusion has a relatively firm theoretical base, which requires only the input of an experimentally determined velocity profile to allow theoretical predictions. Such an opportunity, to compare theory and experiment, is rare in the field of turbulent mixing. The success of vertical turbulent diffusion theory is surveyed in §1.2.

The dispersion experiments described in this paper were all undertaken in the flow region where both vertical and lateral mixing were occurring simultaneously. For this reason a theoretical basis for the determination of the lateral diffusivity in this near-field mixing zone is presented in §2. The experimental set-up and apparatus are detailed in §3, while the experimental results are summarized and discussed in §4.

1.1. *Lateral mixing*

Considerable experimental effort has been invested in the determination of the depth-averaged lateral diffusivity $\bar{\epsilon}_z$, for straight, rectangular laboratory channels. The first two substantial studies dedicated to this end were undertaken by Okoye (1970) and Prych (1970). Okoye performed a large number of experiments in flows with a variety of aspect ratios (depth/width) and friction factors and concluded that $\bar{\epsilon}_z$, non-dimensionalized by the shear velocity and the flow depth, correlated with the aspect ratio, tending to decrease as the aspect ratio increased. His values of $\bar{\epsilon}_z/u_* d$ varied between 0.09 and 0.235. While the main thrust of Prych's study was to understand the effect of density differences between the effluent and the ambient fluid on lateral mixing, he did perform a number of experiments with no density difference. His results demonstrated that $\bar{\epsilon}_z/u_* d$ lay within the range 0.136 to 0.162.

Miller & Richardson (1974) published the results of experiments performed in flows with an almost constant aspect ratio of 0.21. The values of $\bar{\epsilon}_z/u_* d$ they obtained varied between 0.10 and 0.18, depending on the value of the friction factor. It should be noted that, because of their relatively large aspect ratios, their flows were strongly three-dimensional.

While steady tracer sources were used in the experimental programmes already described, Sullivan (1971) investigated the longitudinal and lateral mixing characteristics of a blob of tracer. He obtained values of 0.108, 0.110 and 0.133 for the non-dimensional lateral diffusivity in a channel with an aspect ratio of less than 0.125.

In an attempt to draw all the published data into a coherent whole Lau & Krishnappan (1977) published a comprehensive review paper containing the results of the lateral dispersion studies performed to that date. To the results of the nine studies examined they added the results of their own work. No consistent trend in the variation of $\bar{\epsilon}_z/u_* d$ with aspect ratio was found throughout these ten studies: with the exception of those of Lau & Krishnappan, all the results are presented in figure 1. This large scatter prompted Lau & Krishnappan to reanalyse the results by non-dimensionalizing by the flow width w, instead of the flow depth. The resulting variation of $\bar{\epsilon}_z/u_* w$ with aspect ratio is demonstrated in figure 2. In conclusion Lau

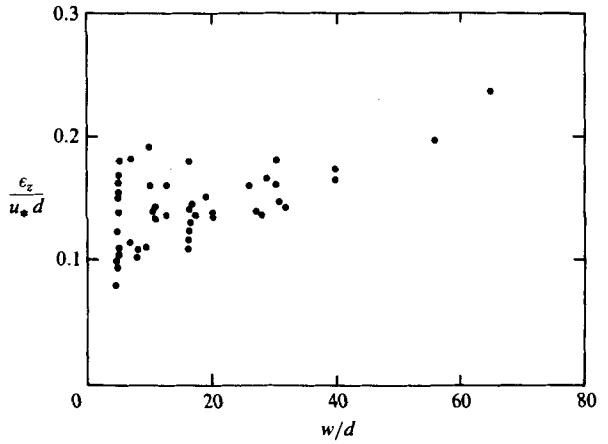

FIGURE 1. The non-dimensional lateral diffusivity plotted against the ratio of channel width to flow depth for the experimental results of the studies reviewed in Lau & Krishnappan (1977).

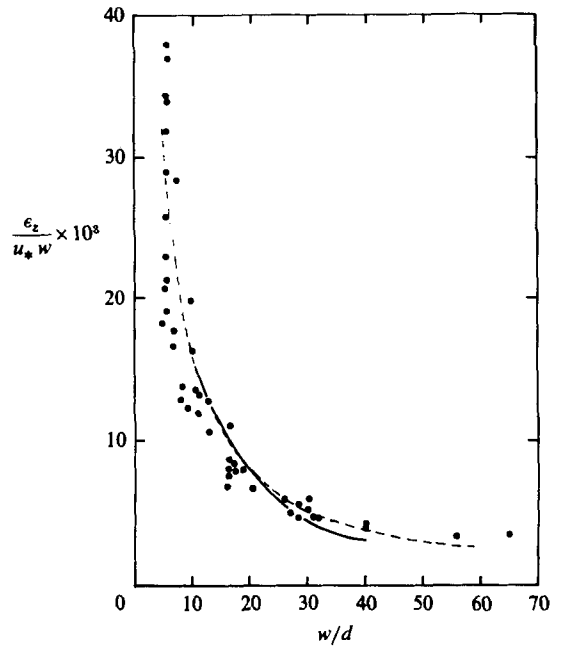

FIGURE 2. The non-dimensional lateral diffusivity plotted against the ratio of flow width to flow depth. The experimental data points are the same as those referred to in the caption to figure 1 while the solid curve represents the trend of the results of Lau & Krishnappan (1977). Following the suggestion of one of the referees the dashed line, representing the function $\bar{\epsilon}_z/u_* w = 9.16/(w/d)$, is also included in this figure. It demonstrates the fit to the data obtained when the non-dimensional lateral diffusivity is independent of the flow width: a result inconsistent with Lau & Krishnappan's conclusion.

& Krishnappan deduced that $\bar{\epsilon}_z/u_* w$ was the better non-dimensionalization and that the principal mixing mechanism in straight rectangular channels, therefore, was not turbulence but secondary currents.

However, the results of a study by Webel & Schatzmann (1984) were at variance with the conclusions of Lau & Krishnappan. Their experimental programme

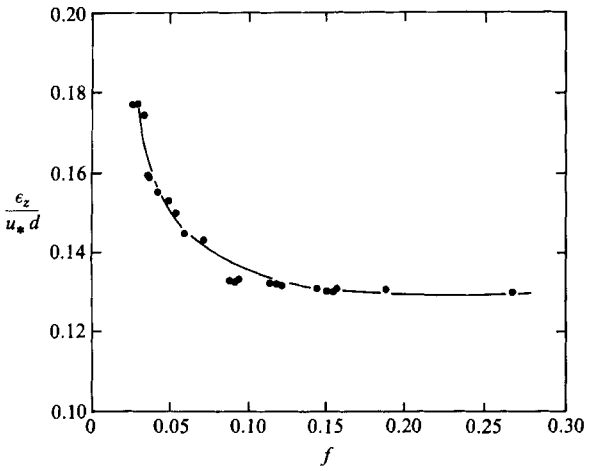

FIGURE 3. The experimental results of Webel & Schatzmann (1984).

included a total of more than 80 runs with flows of varying Froude number, Reynolds number, friction factor and aspect ratio. The results demonstrated that $\bar{\epsilon}_z/u_* d$ was independent of each of these parameters with the exception of the friction factor. For values of f greater than 0.08 the value of $\bar{\epsilon}_z/u_* d$ was about 0.13, but below this value the non-dimensionalized diffusion coefficient gradually increased up to a value of approximately 0.17 for smooth-bed flows with a friction factor of about 0.02. Figure 3 presents their results. Webel & Schatzmann concluded that the flow depth, and not the flow width, was the correct lengthscale of the lateral mixing process and that, therefore, turbulent mixing was by far the most important mixing mechanism present.

Clearly, despite the amount of effort invested in the determination of ϵ_z, no consistent trend in the variation of this quantity with the various flow parameters can be deduced from the published results. In fact, in a number of cases the results and conclusions of the various studies are in serious disagreement.

It is worth noting how the values of the lateral diffusivity obtained in the laboratory compare with those obtained in the field. A summary of the results obtained in natural channels may be found in Fischer *et al.* (1979). The values of $\bar{\epsilon}_z/u_* d$ vary from 0.45 to 3.4 in the field experiments, corresponding to mixing rates up to 30 times those measured in the laboratory. The additional mixing mechanisms present in the natural environment must account for this large increase in the mixing coefficient.

1.2. *Vertical mixing*

A number of studies have been dedicated to the theoretical or experimental modelling of two-dimensional vertical dispersion.

Okoye (1970) compared a few of his experimental results to a numerical solution to the diffusion equation, derived by Coudert (1970) using a Crank–Nicholson finite-difference scheme, and found close agreement. Coudert incorporated the realistic logarithmic velocity and parabolic diffusivity profiles in his solution. Yeh & Tsai (1976) and Gabric (1986) solved the same problem using an eigenfunction technique, although they chose power-law representations of the vertical velocity and diffusivity distributions. Robson (1983) also employed an eigenfunction technique and demonstrated the use of variational methods in determining the eigenvalues and

eigenfunctions for this type of problem. Nokes, McNulty & Wood (1984) solved the same problem as that considered by Coudert but, again, employed an eigenfunction-expansion solution to the diffusion equation and derived a full set of eigenvalues and eigenfunctions using a power-series solution. Recently Smith (1985) considered a significantly more general problem, incorporating not only lateral diffusion into the problem but also a vertical drift velocity of a contaminating species with a chemical half-life. His main aim in this paper was to determine the most advantageous vertical positioning of a source of such an effluent.

Experimental studies of vertical dispersion from a steady source are more rare, with those of Jobson & Sayre (1970) and McNulty (1983) being the most notable. Jobson & Sayre performed a series of experiments with a horizontal line source of dye entering the flow at the free surface. They compared their results with their own numerical solution to the vertical diffusion equation, incorporating both the logarithmic velocity and parabolic diffusivity profiles, and found good agreement between the theory and experiment.

McNulty also employed a horizontal line source to allow his salt solution to enter the flow at the free surface or at the channel bed. His modified moment method of solution to the diffusion equation verified that the logarithmic velocity and parabolic diffusivity profiles more accurately model the vertical dispersion process than uniform distributions of these quantities. His results may also be found in Nokes *et al.* (1984) where they are compared with their theoretical solution.

The experimental programme described in this paper was intended to complement these two previous studies in a number of ways. Firstly, the experiments of both Jobson & Sayre and McNulty were performed in rough-bed channels while the experiments described here were undertaken in a smooth-bed channel. Secondly, and more importantly, by using a point source instead of a line source it was possible to position the source in the interior of the fluid without significantly affecting the flow: something that was not feasible with a line source. This enabled a variety of source locations to be examined and, in particular, an experimental check on the location of the ideal source, predicted by theory, to be made.

Okoye (1970) demonstrated the manner in which two-dimensional concentrations can be obtained from the concentration distribution downstream of a point source. Provided the measurements are made in the central region of a wide channel, where the velocity and vertical diffusivity are independent of the transverse coordinate, two-dimensional concentrations can be calculated by integrating the measured point concentrations across the flow. However, care must be taken in the non-dimensionalization of the two-dimensional concentrations, and details of the correct technique may be found in Nokes (1985).

2. Theoretical basis for the determination of the lateral diffusivity in the near-field mixing zone

Starting with the turbulent diffusion equation, Okoye (1970) demonstrated mathematically that (1) below could be used to calculate the depth-averaged lateral diffusivity from the measured lateral concentration profiles, provided the measurements were made downstream of the region in which vertical mixing was taking place:

$$\bar{\epsilon}_z = \tfrac{1}{2}\bar{u}\frac{\overline{\mathrm{d}\sigma^2}}{\mathrm{d}x}, \tag{1}$$

where σ^2 is the variance of the lateral concentration profiles and the overbars denote depth-averaging. However, as one of the reasons for embarking on this experimental programme was the verification of the eigenfunction solution for vertical dispersion (see Nokes *et al.* 1984), the taking of measurements in the near-source region was obligatory.

In order to determine the circumstances under which (1) may be used in the near-source region, and to offer guidance as to how $\bar{\epsilon}_z$ may be evaluated when these conditions are not met, a three-dimensional eigenfunction solution to the turbulent diffusion equation was developed.

The turbulent diffusion equation and its boundary conditions are

$$u(y,z)\frac{\partial c}{\partial x} = \frac{\partial}{\partial y}\left[\epsilon_y \frac{\partial c}{\partial y}\right] + \frac{\partial}{\partial z}\left[\epsilon_z \frac{\partial c}{\partial z}\right], \tag{2}$$

$$\epsilon_y \frac{\partial c}{\partial y} = 0 \quad \text{on } y = 0, y = d, \tag{3}$$

$$\epsilon_z \frac{\partial c}{\partial z} = 0 \quad \text{on } z = 0, z = w, \tag{4}$$

where c is the species concentration, ϵ_y and ϵ_z are the turbulent diffusivities in the y (vertical) and z (transverse) directions respectively and u is the longitudinal velocity distribution. w is the channel width and d its depth. The boundary-layer type approximation, that longitudinal (x) gradients of c are small compared with vertical and transverse gradients, has been made in writing down (2).

Equations (2)–(4) may be conveniently non-dimensionalized by the following transformations:

$$\left.\begin{gathered} x' = \frac{x}{d}, \quad y' = \frac{y}{d}, \quad z' = \frac{z}{d}, \\ u = \bar{u}\chi(y), \quad \epsilon_y = u_* d\psi_y(y), \quad \epsilon_z = u_* d\psi_z(y). \end{gathered}\right\} \tag{5}$$

It should be noted that the choice of non-dimensionalization for ϵ_z is merely the personal preference of the writers. The resulting diffusion equation, where the primes have been dropped for clarity, is

$$\left(\frac{8}{f}\right)^{\frac{1}{2}} \chi \frac{\partial c}{\partial x} = \frac{\partial}{\partial y}\left[\psi_y \frac{\partial x}{\partial y}\right] + \frac{\partial}{\partial z}\left[\psi_z \frac{\partial c}{\partial z}\right], \tag{6}$$

with

$$\psi_y \frac{\partial c}{\partial y} = 0 \quad \text{on } y = 0, y = 1 \tag{7}$$

$$\psi_z \frac{\partial c}{\partial z} = 0 \quad \text{on } z = 0, z = z_0. \tag{8}$$

$f = 8u_*^2/\bar{u}^2$ is the friction factor and z_0 is a non-dimensional width, w/d, equal to the inverse of the aspect ratio.

In the central region of a wide channel, the region in which these experiments were performed, the quantities χ, ψ_y and ψ_z may be assumed to be independent of z and the general solution to (6) may be written as

$$c(x,y,z) = \sum_{n=0}^{\infty} \sum_{m=0}^{\infty} a_{n,m} \cos\left[\frac{n\pi z}{z_0}\right] H_{n,m}(y) \exp\left[-\left(\frac{f}{8}\right)^{\frac{1}{2}} \gamma_{n,m}\, x\right]. \tag{9}$$

$H_{n,m}(y)$ is the mth vertical eigenfunction corresponding to the nth lateral eigenvalue and satisfying (10), and

$$\frac{\mathrm{d}}{\mathrm{d}y}\left[\psi_y \frac{\mathrm{d}H_{n,m}}{\mathrm{d}y}\right]+\left[\gamma_{n,m}\chi-\frac{n^2\pi^2}{z_0^2}\psi_z\right]H_{n,m}=0. \tag{10}$$

$\gamma_{n,m}$ are the associated vertical eigenvalues and $a_{n,m}$ are the expansion coefficients obtained from the source condition, $c(0,y,z)=c_s(y,z)$, and the orthogonality of the eigenfunctions:

$$a_{n,m}=\frac{\displaystyle\int_0^{z_0}\int_0^1 \chi c_s H_{n,m}(y)\cos\left[\frac{n\pi z}{z_0}\right]\mathrm{d}y\,\mathrm{d}z}{\displaystyle\int_0^1 \chi H_{n,m}^2\,\mathrm{d}y\int_0^{z_0}\cos^2\left[\frac{n\pi z}{z_0}\right]\mathrm{d}z}. \tag{11}$$

2.1. *Coupling between the diffusion processes*

The mathematical terms representing all three mixing mechanisms, vertical and lateral diffusion and advection, are present in (10) and a coupling between the two diffusion processes has been noted by the fact that the vertical eigenfunctions depend on the value of the lateral eigenvalue. This dependence ensures that the vertical mixing process varies with position across the flow and it arises from the different forms of χ and ψ_z in the second term in (10).

The physical cause of this coupling is straightforward. Suppose, for example, that the lateral diffusivity is independent of y, then, as the advection rate increases with height in the flow, the spread of the plume near the top of the flow (a high-velocity region), measured at a particular value of x, will be less than that of the plume near the channel bed (a low-velocity region). This is simply because the slow-moving material near the bed has taken longer to arrive at the particular downstream location than its faster-moving counterpart, and thus it has had longer to diffuse laterally. If a vertical line source is placed in the flow, vertical gradients will be established in the plume where no such gradients existed originally. It can be reasoned that near the edge of the plume the vertical transfer of material will be upwards while near the centre this transport will be in the opposite direction. In both instances the vertical diffusion attempts to 'iron out' the vertical gradients caused by the lateral diffusion.

Only for the rather special case, when χ and ψ_z have the same vertical dependence, does the coupling disappear from the problem. In this case the increase of the lateral diffusion coefficient with height above the channel bed exactly compensates for the increasing advection rate, and the apparent rate of lateral spreading is independent of height.

2.2. *The effect of coupling on the calculation of* ϵ_z

Near the source this coupling of the two diffusion processes will affect the value of ϵ_z deduced from the measured spreading of the plume. To investigate the significance of this effect three mathematical solutions to (6), using the eigenfunction expansion already described, were produced, incorporating three different forms of ψ_z. All three solutions used a power-law velocity distribution (see Nokes *et al.* 1984 for the justification of this) and a parabolic vertical diffusivity which took the following forms:

$$\chi(y)=(1+\alpha)y^{\alpha}, \tag{12}$$

$$\psi_y(y)=\kappa y(1-y). \tag{13}$$

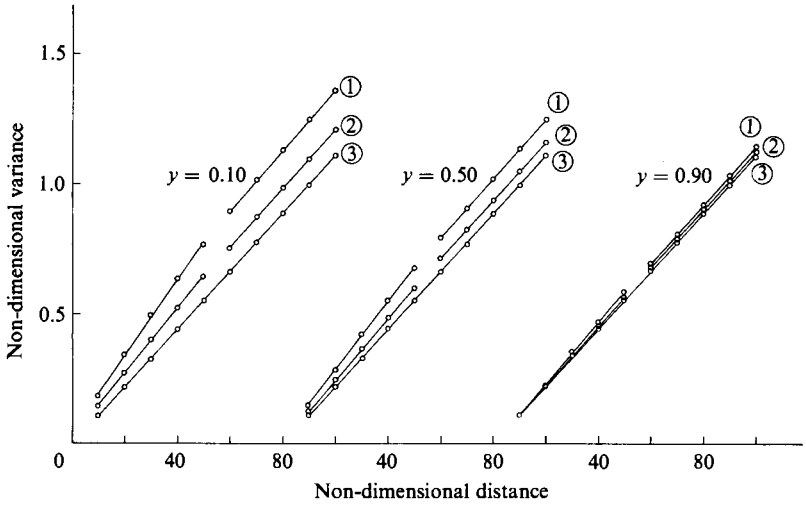

FIGURE 4. Non-dimensional variance of the theoretically determined lateral concentration profiles plotted against non-dimensional distance from the source. The source is at $y_s = 0.05$ and $z_s = 4.30$ and the other flow parameters are $f = 0.0243$, $\alpha = 0.15$, $\kappa = 0.4$, $z_0 = 8.6$ and $\bar{\psi}_z = 0.10$. Curve 1, ψ_z linear; curve 2, ψ_z uniform; curve 3, ψ_z power distribution.

The power-law velocity distribution was derived from a least-squares best fit to the logarithmic velocity distribution corresponding to particular values of f and κ (von Kármán's constant). The three distributions of ψ_z used were

$$\psi_z(y) = 0.1(1+\alpha)\, y^{\alpha} \quad \text{(power)}, \tag{14}$$

$$\psi_z(y) = 0.1 \quad \text{(uniform)}, \tag{15}$$

$$\psi_z(y) = 0.1\frac{4-2y}{3} \quad \text{(linear)}. \tag{16}$$

In all three cases the vertical eigenfunctions were evaluated with the power-series solution technique detailed in Nokes *et al.* (1984).

Figure 4 illustrates the growth of the non-dimensional variance of the lateral concentration profiles at three levels in the flow, for each of the three eigenfunction solutions. The source is at $y = 0.05$. Values of $\mathrm{d}\sigma^2/\mathrm{d}x$ for the calculations between $x = 10$ and $x = 50$, and those between $x = 60$ and $x = 100$ are tabulated in table 1. Also included in this table are the values of $\bar{\psi}_z$ calculated from the non-dimensional form of (1) using the three calculated values of $\mathrm{d}\sigma^2/\mathrm{d}x$, and these may be compared with the value of 0.10 used in the theoretical computations.

The uncoupled solution (ψ_z given in (14)) yields the correct value of $\bar{\psi}_z$ and, as expected, the growth rate of the variance is independent of the sampling level and position downstream of the source. In fact, any of the measured values of $\mathrm{d}\sigma^2/\mathrm{d}x$ could be used in (1) to obtain the correct value of $\bar{\psi}_z$.

However, the two coupled solutions exhibit quite different behaviour. For the purposes of the following discussion only the case of a linear distribution of the lateral diffusivity will be considered as the uniform distribution demonstrates similar, if less extreme, behaviour. At $y = 0.1$ the coupled solution predicts that the variance grows more rapidly with x than is predicted by the uncoupled solution. This is true for all levels in the flow although the difference between the two solutions decreases as the sampling level approaches the surface. Near the channel bed the

$\frac{d\sigma^2}{dx}$	Lateral diffusivity		
	Linear	Uniform	Power
Sampling level			
0.1 (*a*)	0.0145	0.0124	0.0110
(*b*)	0.0116	0.0112	0.0110
0.5 (*a*)	0.0132	0.0119	0.0110
(*b*)	0.0113	0.0112	0.0110
0.9 (*a*)	0.0119	0.0115	0.0110
(*b*)	0.0112	0.0111	0.0110
$\bar{\psi}_z$ (*a*)	0.120	0.108	0.100
(*b*)	0.103	0.101	0.100

TABLE 1. The slopes of the curves drawn in figure 4. The value of $\bar{\psi}_z$, at the bottom of each column, was calculated from (1) using the values of $d\sigma^2/dx$ presented in this table. The results between $x = 10$ and $x = 50$ are designated by (*a*), and those between $x = 60$ and $x = 100$ by (*b*).

linear distribution is greater than the uncoupled power profile and thus the plume spreads more rapidly. However, at a sampling level near the free surface the dispersing material has sampled the velocity and lateral diffusivity at nearly all levels in the flow, approximately averaging them. Therefore at $y = 0.90$ all distributions of ψ_z predict similar values of $d\sigma^2/dx$.

It should be noted also that the discrepancy between the predictions of the coupled and uncoupled solutions decreases with distance from the source. This is because vertical mixing is approaching completion by $x \approx 60$. At this point in the flow, where essentially no vertical gradients exist, the rate of lateral spreading is independent of height and must represent some flow average. As deduced by Okoye (1970), in this region, far from the source, (1) may be used to calculate $\bar{\epsilon}_z$ for any vertical distribution of the lateral diffusion coefficient.

In the near-field region ($0 \leqslant x \leqslant 50$) the deduced value of $\bar{\psi}_z$ depends markedly on the chosen distribution of ψ_z. The linear distribution predicts a value of $\bar{\psi}_z$ 20% greater than the true value.

Similar computations were performed for a source placed at $y = 0.95$. The source now lies in a low-diffusivity region, when ψ_z is assumed linear, and the deduced value of the depth-averaged diffusivity, calculated from the near-source measurements, is 12% lower than the true value.

These theoretical results have important ramifications for the determination of $\bar{\epsilon}_z$ from experiment. In general, (1) cannot be used to determine the depth-averaged lateral diffusivity if concentration measurements are made in the near-source region. However, the results presented above do offer some insight into the manner in which $\bar{\epsilon}_z$ may be estimated from measurements in this region. Two possibilities present themselves. First, a crude estimate of $\bar{\epsilon}_z$ could be obtained by placing the effluent source near one flow boundary while its concentration is monitored near the opposite boundary. This method takes advantage of the rough averaging process already described. It yields values of 0.108 and 0.105 for $\bar{\psi}_z$, for sources at $y = 0.05$ and $y = 0.95$ respectively.

Secondly, while the value of the depth-averaged diffusivity obtained from one source location almost certainly will be in error, the value obtained from an average of the results for a number of source locations should yield a good estimate. Using only the results for the two sources analysed here, and the linear diffusivity, a value

of 0.104 for $\bar{\psi}_z$ is obtained. This 4% error is a significant improvement on the 20% and 12% errors resulting from the use of the measurements for a single source, and, in fact, is probably typical of the experimental errors involved in determining the diffusion coefficient from (1).

Finally, it must be stated that while the measurement of concentrations in the near-source region is disadvantageous, in that (1) is invalid, this is offset to a large extent by the information on the coupling of the vertical and lateral diffusion processes obtained from these measurements. If the growth of σ^2 with x is found to be independent of sampling level and source location, then it may be concluded that χ and ψ_z have the same functional form and (1) may be used throughout the flow. On the other hand, if $\mathrm{d}\sigma^2/\mathrm{d}x$ is sampling-level and source-location dependent, a coupling must exist between the two diffusion processes and an approximate form of ψ_z may be deduced.

3. Experimental set-up and procedures

A total of 9 dispersion experiments were carried out in a 12 m long, 560 mm wide and 430 mm deep tilting flume of rectangular cross-section. Uniform, steady flow was established by adjusting the flume slope, a downstream gate and the discharge entering the flume. The two-dimensionality of the flow was verified by detailed velocity measurements made in one cross-section of the flow and some adjustment of the inflow conditions to the flume were necessary to achieve this. Two pieces of aluminium honeycomb, 8 cm thick with a cell diameter of approximately 1 cm, were placed in the entrance to the channel to straighten the flow and two sheets of fine stainless-steel mesh were placed on the upstream side of each honeycomb to ensure an even discharge across the flume. As will be described later, the clogging of these fine meshes by dirt suspended in the flume water caused problems, and at the completion of the 200 series of experiments two further screens of fine mesh were placed upstream of the configuration already described.

A dilute solution of NaCl was used as the tracer. It entered the flow through one of two stainless-steel, L-shaped tubes of circular cross-section. The tracer was prepared from the flume water immediately before the beginning of an experiment to ensure that the temperature difference between the tracer and the channel water was as small as possible, invariably less than 2 °C. In order the tracer could be treated as a passive scalar quantity the salt concentrations in the tracer needed to be low. A rough guide as to whether the density difference between a tracer and the ambient flow has a significant effect on the dispersion process is given in Fischer *et al.* (1979). For vertical dispersion to be independent of density considerations the following relation must hold:

$$\frac{Q'}{u_*^3 w} \ll 1, \tag{17}$$

while, for density effects to be negligible in lateral dispersion,

$$\frac{Q'}{U_*^3 d} \ll 5, \tag{18}$$

where $Q' = q_e g \Delta\rho/\rho$ and q_e is the effluent discharge and $\Delta\rho/\rho$ the relative density difference between the contaminant and the ambient fluid. For the 200 series of experiments these two non-dimensional parameters had maximum values of 0.28 and 2.4 respectively and for the 300 series (except 301) they had maximum values of 0.16

and 1.8 respectively. Concentration measurements were also analysed to ensure that the density difference between the tracer and the ambient fluid was not affecting the mixing process (e.g. the maximum concentration in the plume was not dropping rapidly to the bed).

Tracer concentrations were measured by withdrawing samples from the flow through a bank of 40 stainless-steel probes and measuring their conductivity with a Radiometer CDC114 flow-through conductivity cell. For the small concentrations of salt used the relationship between conductivity and concentration was linear. As only a limited number of samples could be gathered and analysed with the equipment available, the gathering of results, for one complete experimental run, required three separate days of experimentation.

3.1. *Measurement error*

Errors in the measurement took two forms. First, the measured conductivities could be in error owing to residues left in the test-tubes (in which the samples were stored for analysis) after cleaning. By monitoring the variation of the conductivities of the flume water an estimate of ± 0.3 μS/cm for this measurement error was obtained.

Secondly, errors arose from the positioning of the probes in the flow and the finite size of the probes themselves. Slight variations in the flow depth, due to unevenness in the flume bed, also caused an uncertainty in the vertical positioning of the probes and it was estimated that contributions from all of these sources resulted in an error in the vertical position of each probe of 2 mm above and below its mean position. This error is incorporated into the vertical dispersion results presented in §4.

Both of the sources of error discussed above affected the calculation of the variances of the lateral concentration profiles, used in the evaluation of the lateral diffusivity coefficient. In order to obtain a rough estimate of the error in the calculated variances, due to the measurement uncertainties, a computer simulation of the experimental error was undertaken. This was achieved by superimposing random experimental error on the measured concentrations and recalculating the variance of the lateral profile. Random errors were estimated for the measured conductivities and the lateral positioning of the probes. Errors in the vertical probe positions which, in a region of significant vertical gradients, would also affect the calculated variances, were not simulated.

This process was repeated 100 times for each lateral profile, and from these simulated profiles a value for the standard deviation of the simulated variances was calculated. A value of twice this standard deviation was used as an estimate for the error in the variance.

While a randomly imposed error is somewhat less physical than a Gaussian distribution of error it was felt that, as the simulated errors were only rough estimates, the simulation described was adequate.

4. Experimental results

Dispersion experiments were conducted in two smooth-bed flows with a variety of source locations. As was described in §§1 and 2 the ability to adjust the vertical position of the tracer source was of interest for both the vertical and lateral dispersion processes analysed here. Table 2 presents the essential hydraulic data for each flow and dispersion run.

Flow	d (m)	w (m)	d/w	$\bar{u}$ (m/s)	u_* (m/s)	S	f	κ	Fr	Re
A	0.065	0.559	0.116	0.281	0.0155	0.00047	0.0243	0.40	0.35	16600
B	0.050	0.559	0.089	0.236	0.0140	0.00047	0.0282	0.34	0.36	10700

	Source			Source	
Run	y_s	z_s	Run	y_s	z_s
201	0.77	4.30	301	0.90	5.59
202	0.23	4.30	302	0.90	5.59
203	0.92	4.30	303	0.24	5.59
204	0.11	4.30	304	0.57	5.59
205	0.38	4.30			

TABLE 2. Hydraulic and dispersion data for all runs. Two flow regimes, A and B, are described in the top table while the position of the tracer sources for each of the dispersion runs is listed in the bottom two tables. The 200 series experiments were conducted in flow A and the 300 series in flow B. The symbols in the tables have the following meanings: d is the flow depth, w the flow width, $\bar{u}$ the mean flow velocity, u_* the shear velocity, S the flume slope, f the friction factor, κ von Kármán's constant, Fr the Froude number, Re the Reynolds number, y_s the non-dimensional height in the flow of the source and z_s the non-dimensional lateral position in the flow of the source. Both y_s and z_s have been non-dimensionalized by the flow depth.

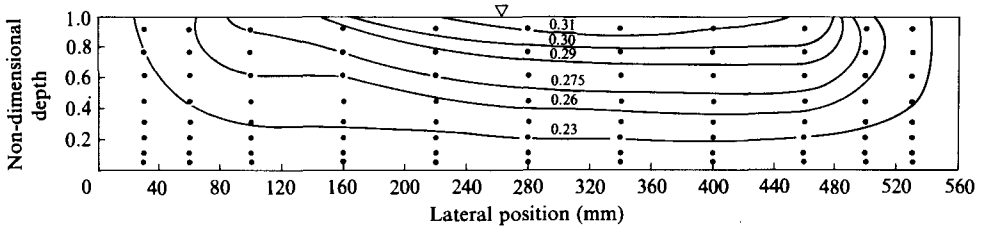

FIGURE 5. Isovels for flow B. All velocities are in m/s. The solid circles mark the points in the cross-section, 6 m downstream of the flume entrance, at which the velocities were measured.

4.1. *Velocity measurements*

For both flows A and B, velocities were measured in the cross-section 6 m downstream of the flume entrance. A plot of the isovels for flow B is presented in figure 5. The curves tracing the lines of constant longitudinal velocity were drawn by eye.

These measured velocities are an important indicator of the presence or absence of secondary currents and lateral velocity gradients in the flow. Both of these phenomena cause additional mixing mechanisms, over and above the natural turbulence driven by the vertical shear, to participate in the dispersion process. The velocity measurements for both flows exhibit a high degree of two-dimensionality over the central region of the channel, a region which terminates 100–140 mm from the flume walls. The depressed velocity maxima in the vertical profiles near the channel walls imply the presence of secondary motions in this region. This feature of the profiles is not evident in the central region of the flow and thus, provided the flow has no significant lateral velocity gradients in this region, secondary circulations are not an important feature.

These observations concur with the calculations of Naot & Rodi (1982) who employed a K–ϵ model in the prediction of secondary currents in turbulent open-

channel flow. Their calculations indicate that, for channels of aspect ratio less than about one quarter, the influence of the secondary circulation is restricted to a region extending approximately two flow depths from the channel walls.

With the exception of the profiles near the walls, the vertical velocity profiles were found to be in fair agreement with the semi-empirical logarithmic velocity law

$$u(y) = \bar{u} + \frac{u_*}{\kappa}[1 + \ln y], \tag{19}$$

where y has been non-dimensionalized by the flow depth. For each profile a least-squares best fit to a logarithmic curve was calculated and from the slope of this curve von Kármán's constant was deduced.

The measured velocities were checked by integrating the velocity over the flow cross-section and comparing this value with the measured value of discharge. For both flows the computed and measured discharges agreed to within 1 %.

4.2. *Two-dimensional concentration distributions*

Longitudinal, two-dimensional concentration profiles were calculated for each run. The results for Run 303 are illustrated in figure 6. Each diagram presents the results for one height in the flow, specified in non-dimensional form in the caption, together with two pairs of theoretical curves. These represent the predictions of two theoretical eigenfunction solutions (see Nokes *et al.* 1984) corresponding to a parabolic diffusivity and logarithmic velocity distribution (solid lines with shading) and a uniform diffusivity and uniform velocity distribution (broken lines) with the same depth-averaged values. In the method of presentation, the error in the vertical positioning of the probes is most naturally incorporated into the theoretical predictions. The two lines for each theoretical solution therefore correspond to the predicted concentrations 2 mm above and below the labelled height in the flow. Only the bulk flow parameters $\bar{u}$, u_* and d together with the measured value of κ and the source height were used in generating the theoretical concentrations.

The mathematical solution incorporating the realistic parabolic diffusivity and logarithmic velocity, denoted the L/P solution hereafter, is seen to be, almost without exception, superior to the second theoretical solution, denoted U/U, in predicting the measured profiles. Particularly encouraging is the ability of the L/P solution to predict the first eigenvalue of the dispersion process, illustrated by the fact that, far from the source, the theoretical and experimental curves decay to the equilibrium value of 1 at virtually the same rate. This rate of decay is considerably more rapid than that predicted by the U/U solution and thus casts doubt on the usefulness of approximating the diffusivity and velocity with these uniform distributions.

As expected the largest discrepancy between theory and experiment occurs close to the source. In this region, where large vertical and lateral concentration gradients exist, any error in probe placement has a considerable effect on the integrated two-dimensional concentration. The source itself also affects the dispersion process immediately downstream, as it introduces another lengthscale into the flow in its immediate vicinity.

In the 200 series it was later found that the wake behind the vertical section of the source probe was enhancing the mixing above the source. For this reason a second source, with a narrower vertical tube, was used for the 300 series of experiments, with the result that the concentration profiles measured above the source demonstrated better agreement with the L/P solution in the later experiments.

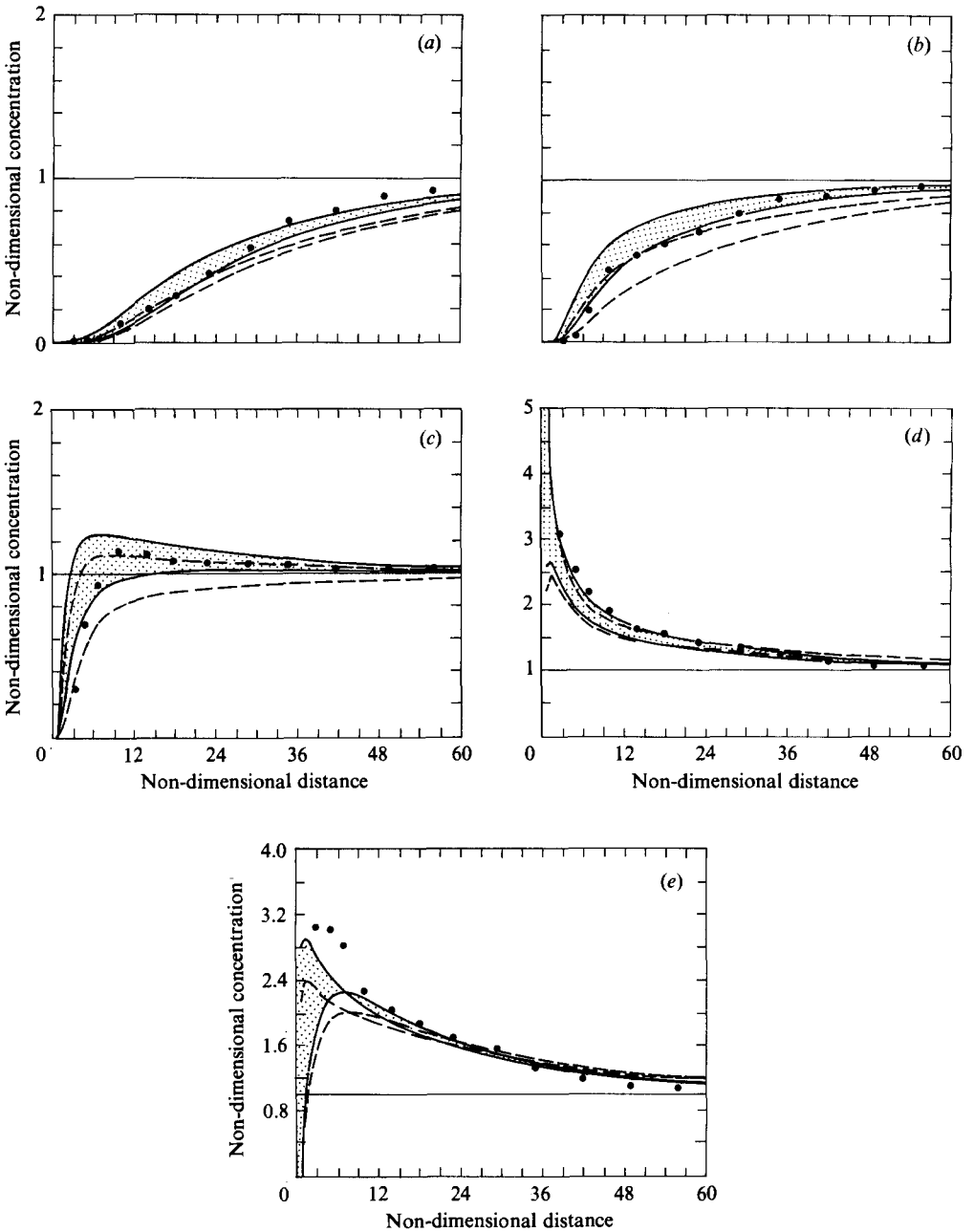

FIGURE 6. Longitudinal profiles of the two-dimensional concentrations for Run 303. Source height = 0.24. (*a*) $y = 0.9$; (*b*) 0.7; (*c*) 0.5; (*d*) 0.3; (*e*) 0.1.

The flexibility obtained by using a point source in the dispersion experiments allows the theoretical prediction of the ideal source location to be verified. The existence of this source position was first demonstrated by Smith (1982) for lateral mixing and extended to vertical mixing by Nokes *et al.* (1984). The ideal source location corresponds to the zero of the first eigenfunction, and theory predicts that

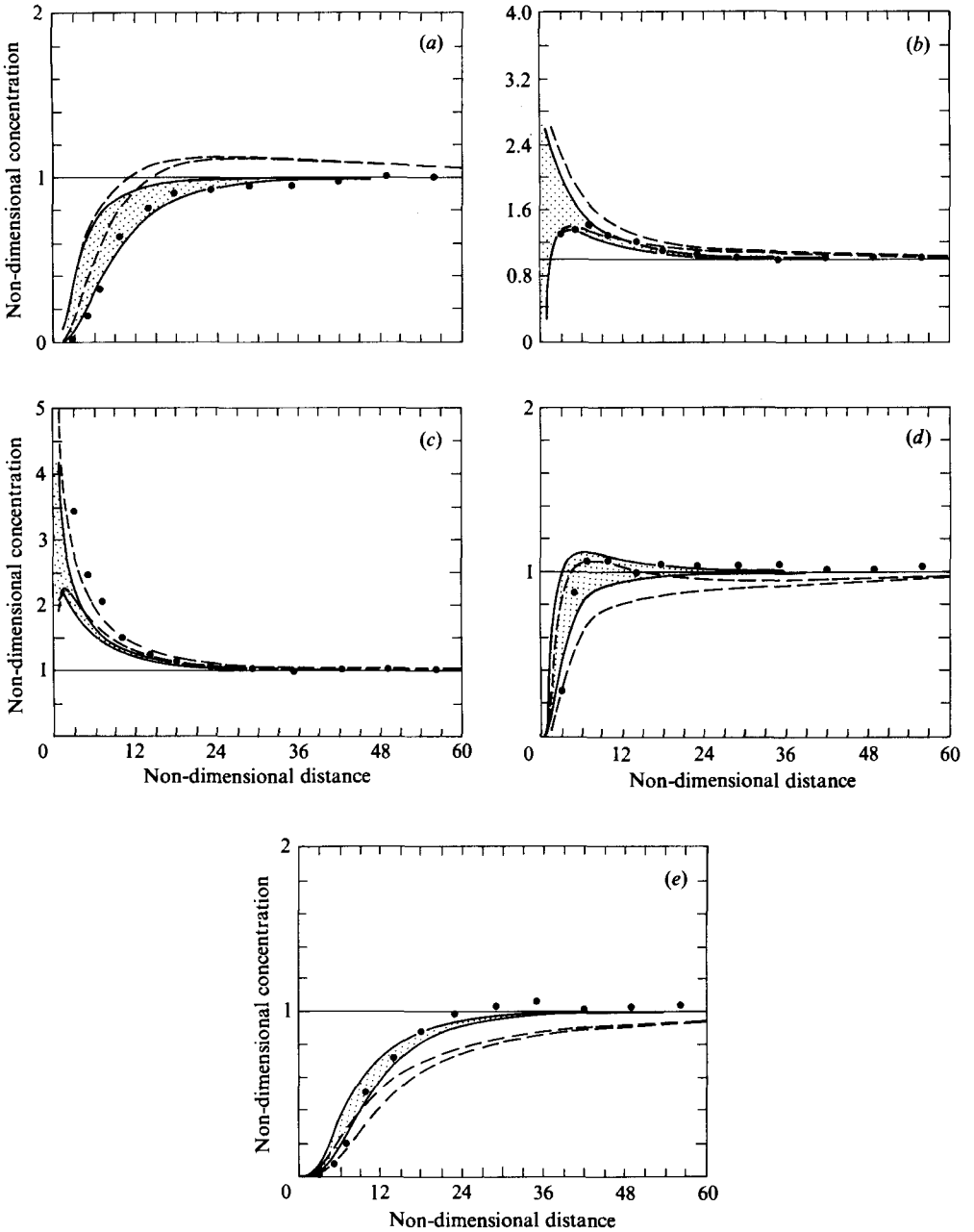

FIGURE 7. Longitudinal profiles of the two-dimensional concentrations for Run 304. Source height = 0.57. (*a*) $y = 0.9$; (*b*) 0.7; (*c*) 0.5; (*d*) 0.3; (*e*) 0.1.

the plume emitted from this position will travel horizontally in the flow: the maximum concentration neither rising to the surface nor dropping to the bed. Run 304 was performed with the source at the theoretically determined ideal source position, $y = 0.57$. Figure 7 presents the results for this run. As for the previous runs the L/P solution models the dispersion process remarkably well. The rapid approach

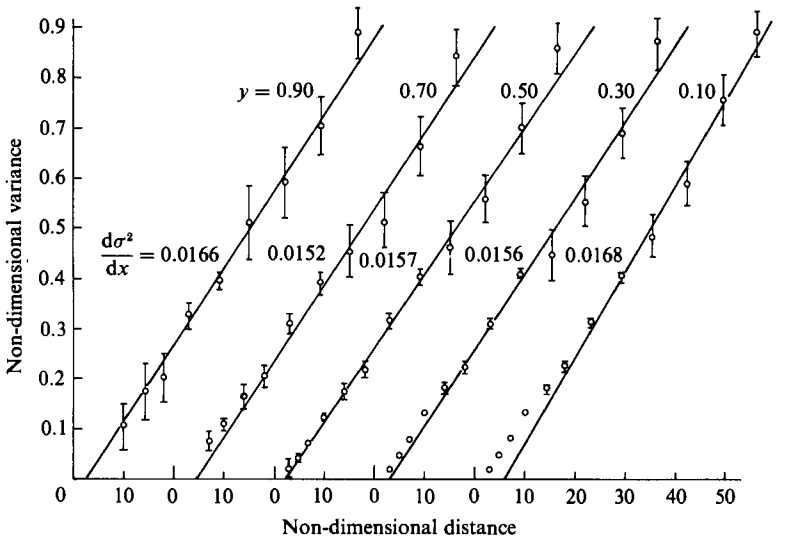

FIGURE 8. The growth of variance with x for five heights in the flow: Run 303. The error bars represent simulated errors.

to equilibrium, predicted by theory, is confirmed by experiment and only a very slight movement of the concentration maximum to the flume bed can be detected. The U/U solution predicts that this maximum will rise to the free surface and, therefore, that much slower mixing will take place. Certainly the success of the L/P solution in predicting the ideal source location serves to confirm the correctness of the parabolic diffusivity and logarithmic velocity profiles.

4.3. *The lateral diffusivity*

The growth of the variance of the lateral concentration profiles with distance from the source is illustrated in figure 8. The errors shown in the figure are those estimated from the computer simulation described in §3.1.

For all runs the growth of σ^2 with x did not become linear until the plume had travelled 8–10 depths downstream of the source. In this near-source region the variance grew more slowly than at greater distances downstream, an effect that can be found in the results of Okoye (1970) also. A possible reason for the presence of this slow-mixing region is the inability of the larger eddies in the flow, the principal mixing mechanism, to break the plume apart as it leaves the source. In addition, the introduction of another lengthscale into the flow, due to the presence of the source probe, will affect the mixing characteristics near the source.

For the data points lying in the linear region a least-squares best-fit line was calculated. The slopes of these lines are summarized in table 3.

Significant deviation from the linear dependence of σ^2 on x occurred in Runs 202 and 205. In the case of Run 205 the points obtained on different days (three days were required to complete one experimental run) lay on distinct lines, even though the slopes of these lines were similar and the figures appearing in table 3 are averages of these two slopes.

The results for Run 202 are of particular interest. They are presented in figure 9. After the results for the first eight downstream locations had been gathered, it was found that the fine mesh screens in the inlet configuration were somewhat clogged by dirt suspended in the flume water and these were cleaned before continuing with the

Run	y_s	$\frac{d\sigma^2}{dx}$ $y = 0.85$	$y = 0.69$	$y = 0.46$	$y = 0.31$	$y = 0.15$	$\bar{\epsilon}_z/u_* d$
201	0.77	0.0242	0.0237	0.0228	0.0225	0.0214	0.208
202	0.23	0.0143	0.0135	0.0128	0.0125	0.0128	0.120
203	0.92	0.0107	0.0104	0.0108	0.0108	0.0105	0.096
204	0.11	0.0163	0.0163	0.0156	0.0155	0.0149	0.143
205	0.38	0.0139	0.0148	0.0146	0.0146	0.0145	0.132

Excluding Run 201 Flow A mean $\bar{\epsilon}_z/u_* d = 0.123$.

Run	y_s	$\frac{d\sigma^2}{dx}$ $y = 0.90$	$y = 0.70$	$y = 0.50$	$y = 0.30$	$y = 0.10$	$\bar{\epsilon}_z/u_* d$
301	0.90	0.0148	0.0147	0.0152	0.0153	0.0135	0.127
302	0.90	0.0156	0.0150	0.0150	0.0144	0.0150	0.130
303	0.24	0.0166	0.0152	0.0157	0.0156	0.0168	0.135
304	0.57	0.0155	0.0153	0.0157	0.0160	0.0163	0.133

Flow B mean $\bar{\epsilon}_z/u_* d = 0.131$.

TABLE 3. A summary of the experimental values of $d\sigma^2/dx$ for all runs. The lateral spreading of the plume was measured at five heights in the flow. A depth-averaged value of $\epsilon_z/u_* d$ is given for each run and a mean value is listed for each flow regime.

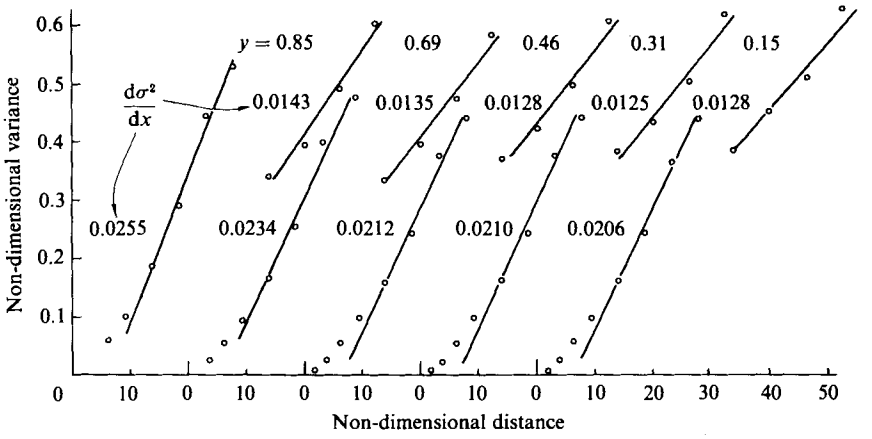

FIGURE 9. The growth of variance with x for five heights in the flow: Run 202.

measurements at the last four stations. The dramatic effect of cleaning the screens is readily seen. The rate of growth of variance with x, for the results obtained after the screens had been cleaned, is barely 60% of that beforehand. Run 201 was conducted before the screens had been cleaned also and it had similarly high slopes. To avoid problems of this nature the inlet screens were thoroughly cleaned after each day's measurements, and two further fine screens were added to the inlet conditions to prevent any clogging in the more important downstream meshes.

It seems reasonable to conclude that the clogged screens caused an irregularity in the discharge across the flow, thus setting up lateral velocity gradients that persisted far downstream of the flume entrance. These gradients in turn generated turbulence, independent of the vertical shear, which enhanced the mixing of the tracer. This

conclusion has important ramifications if experimentally obtained values for $\bar{\epsilon}_z$, from different studies, are to be compared, a point discussed in detail later in this section.

Certainly the inflow conditions to a flume have a significant effect on the mixing characteristics of the flow, although this effect is magnified in a smooth-bed flume where the turbulence generated by the vertical shear is rather weak. It would be expected that this sensitivity to the inflow conditions would be somewhat less in a rough-bed channel with its increased turbulent intensity.

A further interesting feature of this phenomenon is that, while the entry conditions dramatically affect the lateral spreading of the tracer, the vertical mixing process is totally unaffected. The two-dimensional concentrations, calculated before and after the cleaning of the screens, are quite consistent and no discontinuity, similar to that in figure 9, can be detected. This result leads to the general conclusion that the vertical and lateral dispersion processes are almost totally independent. While the inflow conditions may cause irregularities in the vertical turbulent structure, it appears that these irregularities decay quite rapidly and are dominated by the turbulence generated by the vertical shear.

In the theoretical part of this paper, §2, it was noted that (1), in general, could not be used to determine $\bar{\epsilon}_z$ except in the special case when the growth of variance with x was not dependent on source height and sampling level. While the values of $\mathrm{d}\sigma^2/\mathrm{d}x$ for a particular flow may vary somewhat with source location no consistent trend can be seen in the results for flows A and B. In addition to this, no significant variation in $\mathrm{d}\sigma^2/\mathrm{d}x$ with sampling level can be found in any of the runs and again no trend in a variation of this nature can be found throughout all of the runs. This result leads to the conclusion that, to within experimental uncertainty, the growth of σ^2 with x is independent of source height and sampling level and, therefore, the two diffusion processes are essentially uncoupled. The results of Okoye (1970) suggested that the lateral diffusivity had a maximum near the free surface and decreased towards the channel bed. These observations are consistent with the results of this study.

It seems reasonable that ϵ_z should have a similar vertical variation to the velocity distribution, for both the velocity and horizontal eddies must vanish at the bed but are essentially unrestricted at the free surface.

The lack of coupling between the vertical and lateral diffusion processes implies that (1) may be used to determine $\bar{\epsilon}_z$ for each run. This quantity, non-dimensionalized by the flow depth and shear velocity, is also listed in table 3, together with an average value for each flow. It should be noted that the results for Run 201 were not included in the calculation of the average for flow A and the slopes quoted for Run 202 are those measured after the cleaning of the screens.

The results for flow A show a considerable spread and the value of the non-dimensional diffusion coefficient for Run 203 is particularly low. On the other hand, the four 300 series experiments all yield values of $\bar{\epsilon}_z/u_* d$ within 4% of the average value of 0.131. It is no surprise that the results for flow B are more consistent than those for flow A as the extra screens had been incorporated in the inlet conditions and the importance of clean screens was more fully appreciated during the 300 series.

4.3.1. *A comparison with previous studies*

It has already been mentioned in the brief literature review, given in §1.1, that previous studies on lateral mixing have shown a remarkable inconsistency in their findings.

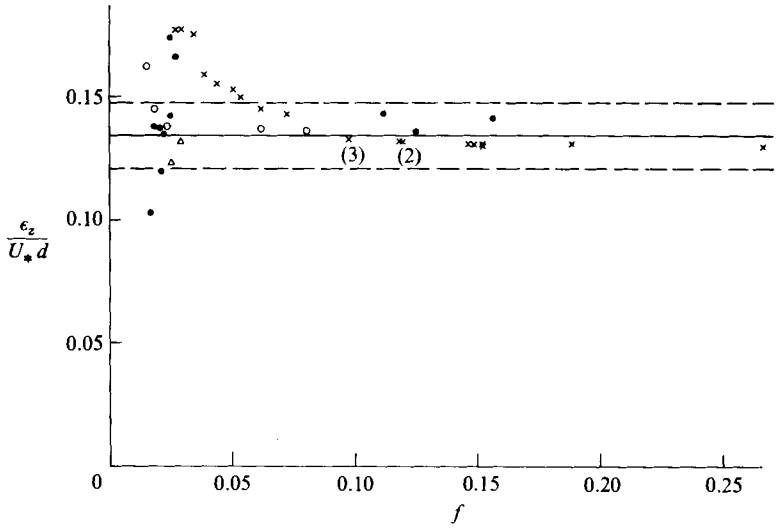

FIGURE 10. The non-dimensional lateral turbulent diffusion coefficient as a function of friction factor. Results from a number of studies are presented. The solid line corresponds to an approximate mean of 0.134 and the dashed lines represent an error of $\pm 10\%$ of this value. ●, Okoye (1970) (selected); ○, Prych (1970); ×, Webel & Schatzmann (1984); △, present study.

A decision must be made as to whether the lateral mixing coefficient is in fact a turbulent diffusion coefficient or a 'catch all' parameter that includes the effects of secondary currents, density currents, changes in channel geometry, etc. Consistency in the results for ϵ_z can be expected only if all experimental studies are performed with the same mixing mechanisms present in the flow.

Therefore, it is proposed that ϵ_z only refer to the lateral spreading due solely to turbulence generated by the floor or horizontal boundaries in a wide channel. To decide whether, in fact, this is the only mixing mechanism present in a particular flow, the measured velocities must confirm the two-dimensionality of the flow in the region over which the plume is spreading.

The results of Prych (1970), Okoye (1970), Miller & Richardson (1974), Lau & Krishnappan (1977), the four most important studies quoted by Lau & Krishnappan in their review paper, and those of Webel & Schatzmann (1984) were reconsidered in the light of the proposed definition of ϵ_z. The experiments of Miller & Richardson were performed in highly three-dimensional flows (aspect ratio ≈ 0.2) and large lateral velocity gradients were present throughout their flows, as illustrated by their own velocity measurements. These gradients, together with the almost unavoidable secondary currents, would significantly affect the mixing characteristics of their flows. Lau & Krishnappan made no mention of their velocity measurements and their results are not included here.

A number of Okoye's runs were also set aside owing to likely three-dimensional effects. Four of his runs were made with an aspect ratio greater than 0.16 while three further runs were performed in flows with Froude numbers greater than 0.8. Because of the likelihood of the presence of surface waves these runs were also not useful. The remainder of Okoye's runs, together with those of Prych, Webel & Schatzmann and the present study, are presented in figure 10, where the non-dimensionalized lateral diffusivity is plotted against friction factor. The hydraulic data corresponding to the results plotted in figure 10 are listed in table 4.

Researcher(s)	d (m)	u_* (m/s)	$\bar{u}$ (m/s)	f	d/w	$\epsilon_z/u_* d$
Okoye (1970)	0.0275	0.0165	0.300	0.0243	0.0250	0.174
	0.0295	0.0157	0.271	0.0268	0.0347	0.166
	0.0346	0.0176	0.320	0.0243	0.0315	0.142
	0.0525	0.0215	0.424	0.0206	0.0618	0.120
	0.0541	0.0218	0.435	0.0201	0.0492	0.137
	0.0553	0.0220	0.420	0.0219	0.0503	0.135
	0.0681	0.0501	0.359	0.1561	0.0619	0.141
	0.0866	0.0512	0.410	0.1250	0.0787	0.136
	0.1036	0.0505	0.428	0.1115	0.0942	0.143
	0.1070	0.0190	0.418	0.0165	0.1258	0.103
	0.1081	0.0186	0.392	0.0180	0.0983	0.138
Prych (1970)	0.0390	0.0373	0.373	0.080	0.0355	0.136
	0.0640	0.0401	0.459	0.061	0.0582	0.137
	0.0405	0.0190	0.354	0.023	0.0368	0.138
	0.0655	0.0214	0.452	0.018	0.0596	0.145
	0.1110	0.0199	0.460	0.015	0.1010	0.162
Webel &	0.0900	0.0188	0.139	0.146	(*a*)†	0.131
Schatzmann	0.0600	0.0153	0.100	0.188	(*b*)	0.131
(1984)	0.0400	0.0125	0.069	0.266	(*c*)	0.130
	0.0900	0.0188	0.171	0.097	(*a*)	0.133
	0.0600	0.0153	0.126	0.118	(*b*)	0.132
	0.0400	0.0125	0.092	0.148	(*c*)	0.131
	0.0900	0.0149	0.135	0.097	(*a*)	0.133
	0.0600	0.0121	0.100	0.119	(*b*)	0.132
	0.0400	0.0099	0.072	0.152	(*c*)	0.131
	0.0900	0.0115	0.105	0.097	(*a*)	0.133
	0.0600	0.0094	0.077	0.119	(*b*)	0.132
	0.0400	0.0077	0.056	0.152	(*c*)	0.130
	0.0900	0.0115	0.142	0.053	(*a*)	0.150
	0.0600	0.0094	0.108	0.061	(*b*)	0.145
	0.0400	0.0077	0.081	0.072	(*c*)	0.143
	0.0900	0.0115	0.167	0.038	(*a*)	0.159
	0.0600	0.0094	0.128	0.043	(*b*)	0.155
	0.0400	0.0077	0.098	0.050	(*c*)	0.153
	0.0900	0.0073	0.129	0.026	(*a*)	0.177
	0.0600	0.0059	0.100	0.028	(*b*)	0.177
	0.0400	0.0049	0.075	0.034	(*c*)	0.175
Present	0.0650	0.0155	0.281	0.0243	0.1163	0.123
study	0.0500	0.0140	0.236	0.0282	0.0894	0.131

† Webel & Schatzmann altered the width in their channel for each run obtaining the same values of $\epsilon_z/u_* d$ in each case. (*a*) $d/w = 0.0495, 0.0680$; (*b*) $d/w = 0.0330, 0.0452, 0.1235$; (*c*) $d/w = 0.0220, 0.0302, 0.0826$.

TABLE 4. The hydraulic data corresponding to the experimental results presented in figure 10

For rough-bed experiments, $f > 0.055$, all data points lie within less than 10% of the value of 0.134. For a friction factor of less than 0.055 there is considerable scatter. However, it is significant that only one of the 39 data points lies substantially below the value of 0.134. This tends to confirm 0.134 as a lower bound and the values obtained at lower friction factor could be due to problems such as those encountered in Run 202 where small changes in the upstream velocity distribution were not destroyed by the floor-generated turbulence of the smoother channels and greatly affect the value of the non-dimensional dispersion coefficient.

The results of Webel & Schatzmann have demonstrated that $\bar{\epsilon}_z/u_* d$ is independent of aspect ratio and certainly, for friction factors greater than 0.055, all of the results presented show an insensitivity to this parameter. Values of the aspect ratio, corresponding to all of the data points in figure 10, may be found in table 4.

5. Conclusions

The experimental results for vertical dispersion support the use of the eigenfunction solution with a parabolic diffusivity and logarithmic velocity distribution. Using this method, the ideal source location for which the dilution is most rapid is well predicted.

The measurements of the lateral diffusivity in the near-field mixing zone and the three-dimensional eigenfunction solution suggest that the vertical and lateral diffusion processes are uncoupled. This implies that the lateral diffusivity distribution has the same form as the velocity distribution.

The published results for lateral mixing in a long, wide channel imply that the lateral turbulent diffusivity is independent of all flow parameters except the friction factor. When the chief mixing mechanism present is the natural turbulence generated at the floor of a wide channel, the published values of $\bar{\epsilon}_z/u_* d$ all lie near a value of 0.134, except with friction factors less than 0.055. Below this value some scatter exists, but nearly all the values are greater than 0.13. Thus the shear velocity and the flow depth are confirmed as the correct velocity and lengthscales for both vertical and lateral turbulence in wide (aspect ratio $< \frac{1}{8}$) channels.

During the period of this work the first author was supported by the New Zealand University Grants Committee and The National Water and Soil Conservation Authority.

REFERENCES

COUDERT, J. F. 1970 A numerical solution of the two-dimensional diffusion equation in a shear flow. *W. M. Keck Laboratory of Hydraulics and Water Resources, Tech. Memo.* 70-7. California Institute of Technology, Pasadena, CA.

FISCHER, H. B., LIST, E. J., KOH, R. C. Y., IMBERGER, J. & BROOKS, N. H. 1979 *Mixing in Inland and Coastal Waters*, 1st edn. Academic.

GABRIC, A. 1986 An optimal source depth for effluent discharge in turbulent open channel flow. *Mar. Pollut. Bull.* **17**, 63–64.

JOBSON, H. E. & SAYRE, W. W. 1970 Vertical transfer in open channel flow. *J. Hydraul. Div. ASCE* **96**, HY3, 703-724.

LAU, Y. L. & KRISHNAPPAN, B. G. 1977 Transverse dispersion in rectangular channels. *J. Hydraul. Div. ASCE* **103**, HY10, 1173–1189.

MCNULTY, A. J. 1983 Dispersion of a continuous pollutant source in open channel flow. Ph.D. thesis, University of Canterbury, Christchurch, New Zealand, pp. 210.

MCNULTY, A. J. & WOOD, I. R. 1984 A new approach to predicting the dispersion of a continuous pollutant source. *J. Hydraul. Res.* **22**, 23–34.

MILLER, A. C. & RICHARDSON, E. V. 1974 Diffusion and dispersion in open channel flow. *J. Hydraul. Div. ASCE* **100**, HY1, 159–171.

NAOT, D. & RODI, W. 1982 Calculation of secondary currents in channel flow. *J. Hydraul. Div. ASCE* **108**, HY8, 948–968.

NOKES, R. I. 1985 Problems in turbulent dispersion, Ph.D. thesis, University of Canterbury, Christchurch, New Zealand, pp. 229.

NOKES, R. I., MCNULTY, A. J. & WOOD, I. R. 1984 Turbulent dispersion from a steady two-dimensional horizontal source. *J. Fluid Mech.* **149**, 147–159.

OKOYE, J. 1970 Characteristics of transverse mixing in open-channel flows. *W. M. Keck Laboratory of Hydraulics and Water Resources, Rep.* KH-R-23. California Institute of Technology, Pasadena, CA.

PRYCH, E. A. 1970 Effects of density differences on lateral mixing in open-channel flows. *W. M. Keck Laboratory of Hydraulics and Water Resources Rep.* KH-R-21. California Institute of Technology, Pasadena, CA.

ROBSON, R. E. 1983 On the theory of plume trapping by an elevated inversion. *Atmos. Environ.* **17**, 1923–1930.

SMITH, R. 1982 Where to put a steady discharge in a river. *J. Fluid Mech.* **115**, 1–11.

SMITH, R. 1985 Should sewage be discharged at the water surface or near the bed? *J. Fluid Mech.* **152**, 443–454.

SULLIVAN, P. J. 1971 Longitudinal dispersion within a two-dimensional turbulent shear flow. *J. Fluid Mech.* **49**, 551–578.

WEBEL, G. & SCHATZMANN, M. 1984 Transverse mixing in open channel flow. *J. Hydraul. Engng, ASCE* **110**, 423–435.

YEH, G. T. & TSAI, Y. T. 1976 Dispersion of water pollutants in a turbulent shear flow. *Water Resources Res.* **12**, 1265–1270.